Bull Volcanol (2014) 76:856
DOI 10.1007/s00445-014-0856-0

RESEARCH ARTICLE

The influence of porosity and vesicle size on the brittle strength of volcanic rocks and magma

Michael J. Heap · Tao Xu · Chong-feng Chen

Received: 12 February 2014 / Accepted: 3 August 2014

Abstract Volcanic rocks and magma display a wide range of porosity and vesicle size, a result of their complex genesis. While the role of porosity is known to exert a fundamental control on strength in the brittle field, less is known as to the influence of vesicle size. To help resolve this issue, here, we lean on a combination of micromechanical (Sammis and Ashby's pore-emanating crack model) and stochastic (rock failure and process analysis code) modelling. The models show, for a homogenous vesicle size, that an increase in porosity (in the form of circular vesicles, from 0 to 40 %) and/or vesicle diameter (from 0.1 to 2.0 mm) results in a dramatic reduction in strength. For example, uniaxial compressive strength can be reduced by about a factor of 5 as porosity is increased from 0 to 40 %. The presence of vesicles locally amplifies the stress within the groundmass and promotes the nucleation of vesicle-emanating microcracks that grow in the direction of the applied macroscopic stress. As strain increases, these microcracks continue to grow and eventually coalesce leading to macroscopic failure. Vesicle clustering, which promotes the overlap and interaction of the tensile stress lobes at the north and south poles of neighbouring vesicles, and the increased ease of microcrack interaction, is encouraged at higher porosity and reduces sample strength. Once a microcrack nucleates at the vesicle wall, larger vesicles impart higher stress intensities at the crack tips, allowing microcracks to propagate at a lower applied macroscopic stress. Larger vesicles also permit a shorter route through the groundmass for the macroscopic shear fracture. This explains the reduction in strength at higher vesicle diameters (at a constant porosity). The modelling highlights that the reduction in strength as porosity or vesicle size increases is nonlinear; the largest reductions are observed at low porosity and small vesicle diameters. In detail, we find that vesicle diameter can play an important role in dictating strength at low porosity but is largely inconsequential above 15 % porosity. Vesicle clustering and stress lobe interaction are implicit at high porosity, regardless of the vesicle diameter. In the case of an inhomogeneous vesicle size, the microcracks grow from the largest vesicles, and brittle strength is closer to that of the largest vesicle end-member. The results of this study highlight the important role of vesicle size, and the complex interplay between porosity and vesicle size, in controlling the brittle strength of volcanic rocks and magma.

Keywords Porosity · Vesicle size · Volcanic rock · Magma · Brittle strength

Editorial responsibility: A. Gudmundsson

Electronic supplementary material The online version of this article (doi:10.1007/s00445-014-0856-0) contains supplementary material, which is available to authorized users.

M. J. Heap (✉)
Laboratoire de Déformation des Roches, Équipe de Géophysique Expérimentale, Institut de Physique de Globe de Strasbourg (UMR 7516 CNRS), Université de Strasbourg/EOST, 5 rue René Descartes, 67084 Strasbourg, France
e-mail: heap@unistra.fr

T. Xu · C.-f. Chen
Center for Rock Instability and Seismicity Research, Northeastern University, Shenyang 110819, China

Introduction

The genesis of volcanic rocks and magma is a complex and varied process. Ascending magma vesiculates as it depressurises on its journey to the surface (e.g. Sparks 1978; Toramaru 1989; Mangan and Cashman 1993; Navon and Lyakhovsky 1998; Gonnermann and Manga 2012). Viewed simplistically, the rate of ascent (a function of volatile content, crystal content and melt viscosity, amongst others; see Gonnermann and Manga 2012 and references therein) exerts

Published online: 30 August 2014

a fundamental control on the efficiency and extent of outgassing or, in other words, the porosity of the magma. Moderate to fast-ascending magma has little time for outgassing and, as a consequence, can contain a high porosity. By contrast, slow ascending magma has a greater opportunity to outgas and therefore tends to contain a low porosity. This porosity is present as bubbles (in the case of magma) or preserved as vesicles (in the case of volcanic rock). The diameter of the bubbles or preserved vesicles, and their diameter size distribution, depends on numerous interconnected factors including the melt viscosity, the magma volatile content and type and decompression rate, amongst others (e.g. Shea et al. 2010; Gondé et al. 2011; Gonnermann and Manga 2012 and references therein). The consequence of this complex genesis is that the porosity (e.g. Kueppers et al. 1995; see Fig. 1 in Wright et al. 2009) of volcanic rocks and magma can range from almost 0 % to almost 100 % (porosity can be as high as 98 % in the case of reticulite), and their vesicle diameter can span multiple orders of magnitude (typically from a few tens of microns to a few mm; see Shea et al. 2010 and references therein). Experimental studies have exposed the fundamental control of porosity on rock strength in the brittle field (e.g. Chang et al. 2006; Baud et al. 2013), including volcanic rocks (e.g. Al-Harthi et al. 1999; Heap et al. 2014). Initial porosity has also been shown to impact the rheomechanical behaviour of magma (Kendrick et al. 2013). However, less is known as to the influence of vesicle size. This is largely a result of the significant challenge represented by extracting the influence of vesicle diameter on brittle strength for a natural suite of volcanic rocks or bubble size for a suite of vesiculated magma in the laboratory. Not only would sampling a suite of rocks with a wide range of vesicle size prove difficult but also one must minimise other differences that could lead to strength variations, such as crystal content, crystal size, the strength of the glass phase, the presence/absence of microlites and vesicle and/or crystal preferred orientation, amongst many others. While synthetic magma can be fabricated through high-pressure and high-temperature laboratory experiments (e.g. Martel et al. 2001; Caricchi et al. 2011; Laumonier et al. 2011; Pistone et al. 2012), accurately controlling the vesicle diameter during depressurisation remains a challenge. To compound matters, one must accurately measure the vesicle size, a nontrivial task. Measurements can be made, for example, through optical and scanning electron microscopy (destructive), mercury injection (destructive and provides the vesicle throat diameter, not the vesicle diameter) and X-ray or neutron computed tomography (needs to be at a resolution higher than the smallest vesicle size; it can therefore be very expensive to scan large samples). Of the few studies that exist, an increase in pore size (for a given porosity) has been shown to decrease the compressive strength of porous ceramics (Liu 1997). Vasseur et al. (2013) highlighted a potentially important role for vesicle size in reducing the compressive strength of porous lava, using a combination of high-temperature uniaxial experiments on sintered glass samples and micromechanical modelling. However, we note that a numerical study, using a bonded particle model, found that an increase in pore size from 0.5 to 2.5 mm served to increase compressive strength (Fakhimi and Gharahbagh 2011).

In an attempt to better understand the influence of porosity and vesicle diameter on the brittle strength of volcanic rocks and magma, we have performed micromechanical and stochastic modelling in which we systematically varied the porosity and vesicle diameter. While our focus is the brittle strength of volcanic rocks (i.e. edifice rocks, dome rocks that are highly crystallised and/or are at or below the glass transition temperature of their melt phase) and brittle magma (i.e. magma deforming at a strain rate that exceeds the structural relaxation timescale of its melt phase, see Dingwell and Webb 1990; Dingwell 1996), we note that the modelled output of this paper could be applied to any porous, brittle material. The brittle strength of volcanic rocks is of prime importance for edifice stability (Voight 2000); catastrophic flank collapse could ensue if the stability of the edifice is compromised during a period of unrest (e.g. Reid et al. 2010). Faulting within the edifice (and/or at the outermost edge of the conduit where magma can behave in a brittle manner due to the higher strain rates, see Gonnermann and Manga 2003) could facilitate outgassing (e.g. Laumonier et al. 2011; Lavallée et al. 2013; Kendrick et al. 2013) and impact eruption characteristics (effusive or explosive, see Mueller et al. 2008). Further, an enhanced understanding of the brittle failure of porous magma may aid our comprehension of explosive magmatic fragmentation (Zhang 1999; Martel et al. 2001; Spieler et al. 2004).

Description of the models

Micromechanical modelling: Sammis and Ashby's pore-emanating crack model

Micromechanical modelling can provide useful insights in the mechanics of uniaxial compressive failure in brittle materials (Wong and Baud 2012). The pore-emanating crack model, based on fracture mechanics and beam theory, of Sammis and Ashby (1986) describes a two-dimensional elastic medium populated by circular vesicles (that act as stress concentrators for the initiation of extensile cracks) of uniform radius r. As the applied stress (σ) acting on the elastic medium increases, microcracks emanate from the circular vesicles parallel to the direction of the applied stress (in the tensile zones at the north and south poles of the vesicle, as described by fracture mechanics theory) when the stress at the tip of a small microcrack on the vesicle surface reaches a critical value (K_{IC}, the critical stress intensity factor). The formed microcracks propagate to a distance l in the direction of the maximum principal stress. Once the microcracks are long enough, they can interact, thus increasing the local tensile stress intensity (described by an extension of beam theory for closely spaced cracks). Eventually, they coalesce and conspire to induce the macroscopic failure of the elastic medium (Fig. 1). In the case of uniaxial compression, Zhu et al. (2010) derived an analytical approximation of the pore-emanating crack model to estimate uniaxial compressive strength (UCS) as a function of the bulk sample porosity (ϕ):

$$\sigma_{\mathrm{UCS}} = \frac{1.325}{\phi^{0.414}} \frac{K_{\mathrm{IC}}}{\sqrt{\pi r}} \tag{1}$$

Here, the model was run for vesicle diameters of 0.1, 0.2, 0.3, 0.5, 1.0 and 2.0 mm and porosity values of 2, 5, 10, 15, 20, 25, 30, 35 and 40 %. In all cases, we have taken K_{IC} as 1.0 MPa m$^{0.5}$ (we note that changing K_{IC} will just shift the values of UCS and will not change the shape of the curves). A K_{IC} of 1.0 MPa m$^{0.5}$ is similar to that measured for defect-free borosilicate glass (about 0.7 MPa m$^{0.5}$; Wiederhorn 1969). The pore-emanating crack model of Sammis and Ashby (1986) has been previously deployed to understand the mechanics of porous materials, including sandstone (e.g. Baud et al. 2013), limestone (e.g. Zhu et al. 2010), volcanic rocks (e.g. Zhu et al. 2011; Heap et al. 2014) and porous glass (Vasseur et al. 2013).

Stochastic modelling: rock failure and process analysis code (RFPA)

Elastic damage mechanics models have previously been used to study the process of damage accumulation and failure evolution in materials (e.g. Lemaitre and Chaboche 1990). Due to their flexibility, they have been used to simulate a wide range of observations and aid in the understanding of numerous geophysical and engineering problems. For example, such models have been used to understand the progression of rock failure (Tang 1997; Wong et al. 2006), time-dependent deformation (Amitrano and Helmstetter 2006; Xu et al. 2012), coal and gas outbursts in underground collieries (Xu et al. 2006), rockslides (Lacroix and Amitrano 2013), crustal seismic cycles (Tang et al. 2003) and permeability evolution during damage accumulation and failure (Xu and Tang 2008), amongst others. We have implemented a time-independent model so that our model output can be compared with the wealth of existing experimental UCS data (where materials are typically deformed at strain rates of 10^{-5} s^{-1}, i.e. too high to observe significant time-dependent effects). In this study, we adopt the convention that compressive stresses and strains are positive.

The two-dimensional numerical samples of this study—40 mm in length and 20 mm in width—consist of 80,000 square elements with sides of 0.1 mm. The samples are all assigned the same macroscopic physical and mechanical properties (Table 1). These macroscopic properties are considered representative of a sample with 0 % porosity, and, in the absence of microscale heterogeneities, the numerical sample would have a modelled UCS and Young's modulus of 2,300 MPa and 100 GPa, respectively. However, natural samples are rarely uniform and contain defects (microcracks and microlites, amongst others) on the microscale. To reflect material heterogeneity on the microscale, each 0.1-mm square element is assigned a value of strength (compressive and tensile) and Young's modulus using a Weibull probability density function (Weibull 1951):

$$\sigma(u) = \frac{m}{u_0}\left(\frac{u}{u_0}\right)^{m-1} exp\left[-\left(\frac{u}{u_0}\right)^{m}\right] \tag{2}$$

where u is the scale parameter of an individual element, and u_0 is the scale parameter of the average element. Weibull

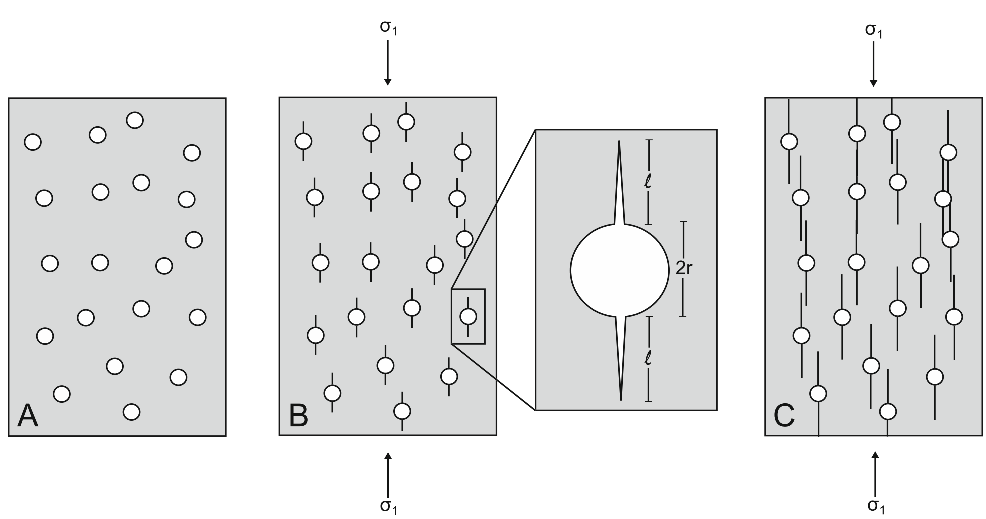

Fig. 1 **a** Two-dimensional elastic medium of Sammis and Ashby (1986) populated by circular voids of uniform radius r. **b** Pore-emanated wing-cracks propagate from the circular voids (to a length l) upon the application of an axial stress (one large enough to overcome K_{IC}). **c** Eventually, as axial stress increases, the wing-cracks grow further, interact and promote macroscopic failure

Table 1 The physical and mechanical properties used in the rock failure and process analysis code (RFPA) stochastic modelling

Homogeneity index	3
Mean uniaxial compressive strength (MPa)	2,300
Mean Young's modulus (GPa)	100
Poisson's ratio	0.25
Ratio of compressive to tensile strength	10
Frictional angle (degrees)	30

distributions have previously been used in numerical modelling (Tang 1997; Xu et al. 2004; Wong et al. 2006; Xu and Tang 2008; Xu et al. 2012) and have successfully captured the process of brittle damage accumulation and failure evolution. The shape parameter *m* (the homogeneity index) reflects the degree of heterogeneity in the numerical sample. The value of *m* describes the distribution of the physical and mechanical properties of the elements about the mean. The distribution is broad for low values of *m* ($m<3$), meaning that the properties of the elements can be very different to that of the mean value; this results in a very heterogeneous sample. The distribution is tight for high values of *m* ($m>10$), meaning that the properties of the elements do not differ greatly from the mean value; this results in a fairly homogenous sample (more information about the *m* parameter is provided in Xu et al. (2012)). We have chosen to let $m=3$ for all of our numerical simulations. A numerical sample with 0 % porosity is shown in Fig. 2a. Each 0.1-mm element is assigned a greyscale value corresponding to the strength of the element (darker colours have values of strength lower than the mean, and vice versa). The modelled output shows that the microscopic heterogeneity serves to lower the UCS (to 553 MPa) of the numerical sample (Fig. 2b). We highlight that the UCS of porosity-free borosilicate glass is about 600 MPa (Vasseur et al. 2013), serving to validate our choice of macroscopic physical and mechanical properties (Table 1) and shape parameter *m*.

We introduced porosity (2, 5, 10, 15, 20, 25, 30, 35 or 40 %) into our numerical samples in the form of circular vesicles. For each value of porosity, we prepared samples that contained vesicle diameters of 0.1, 0.3, 0.5 and 1.0 mm (a total of 36 different combinations). Examples of the numerical samples of porosity 2, 20 and 40 % are given as Fig. 3. To investigate the influence of an inhomogeneous vesicle size distribution on strength, we performed a second set of simulations using numerical samples containing 2 and 40 % porosity with an equal area of 0.1-mm vesicles and 0.3, 0.5 or 1.0-mm vesicles (examples of which are given in Online Resource 1). Vesicles were placed in the samples at random and without overlap. The simulations of this study consider a simplistic system; the rocks or magma do not contain crystals (i.e. the magma is two phase) or pre-existing microcracks greater than 0.1 mm in length.

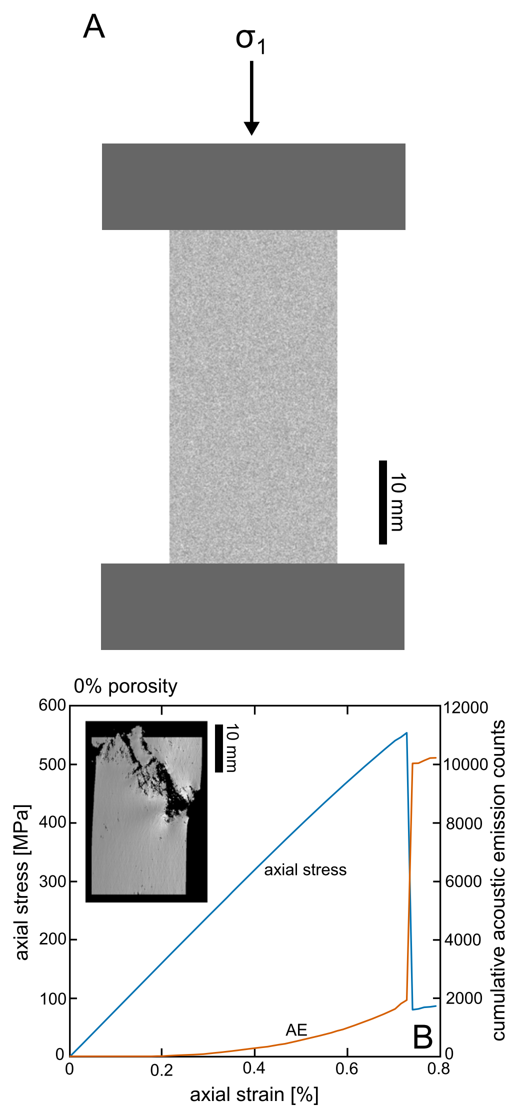

Fig. 2 **a** Numerical sample, 20 mm in width and 40 mm in length, containing 0 % porosity. The upper and lower 'pistons' are represented in *dark grey*. The lower piston remains fixed during the simulations, and the upper piston incrementally moves down to apply strain to the sample. The direction of loading, σ_1, is parallel to the long axis of the sample. **b** The uniaxial stress–strain curve, together with the AE activity, for the sample shown in **a**. The inset shows the final stress field snapshot of the sample

The numerical samples were uniaxially ($\sigma_1>0$ MPa; σ_2 and $\sigma_3=0$ MPa) loaded in 0.002-mm increments until sample failure. Following each uniaxial loading increment, the stress acting upon each element was calculated using the following relation:

$$\sigma_1 = E_0(1-D)\varepsilon_1 \tag{3}$$

where D is the isotropic damage variable, σ_1 is the axial stress, ε_1 is the axial strain, and E_0 is the Young's modulus of an undamaged element. If the stress acting on a particular element met one of the two strength criteria (see below), the

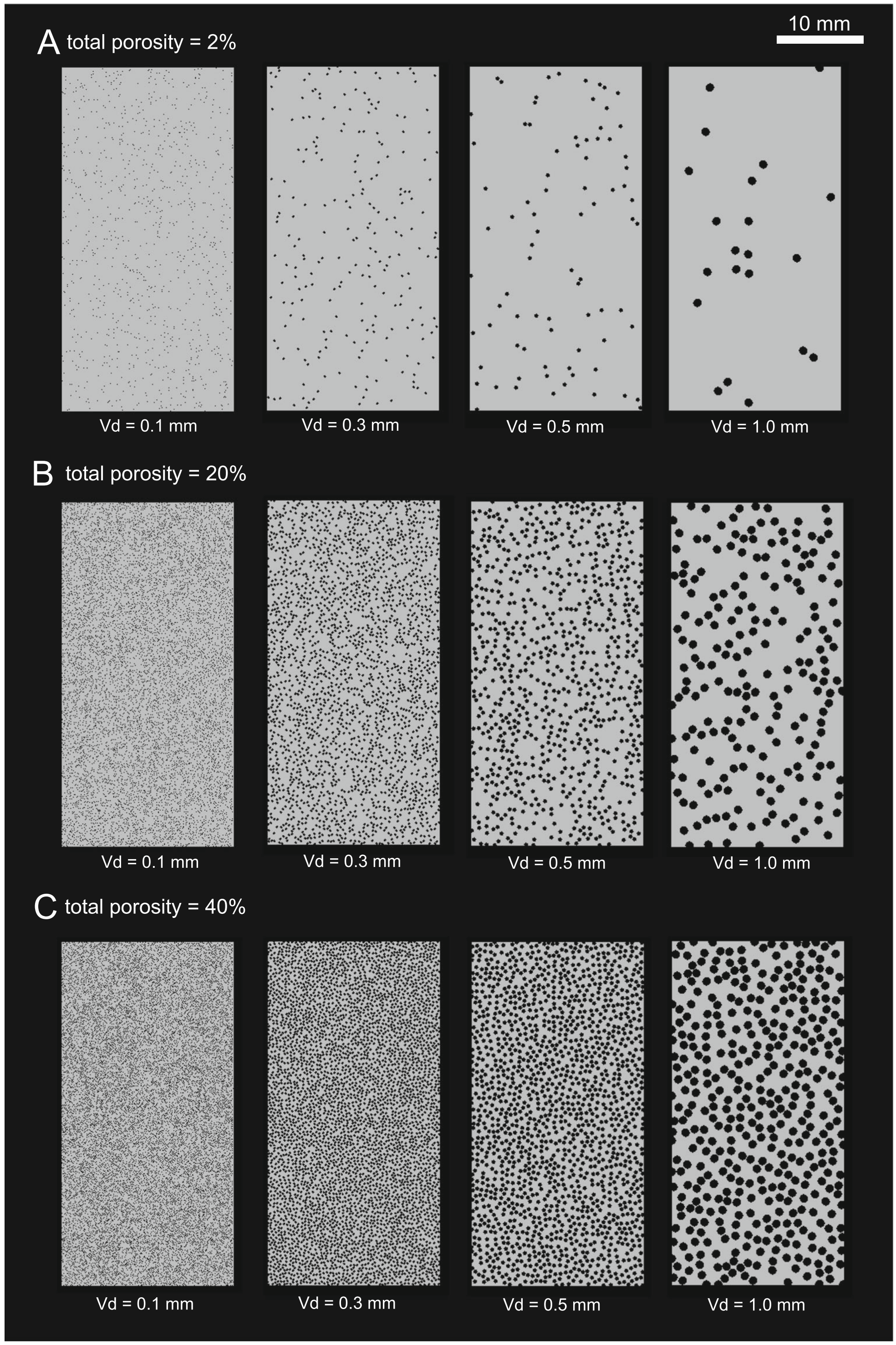

Fig. 3 Examples of the undeformed numerical samples with homogeneous vesicle size distributions used in this study (we use numerical samples containing porosity values of 2, 5, 10, 15, 20, 25, 30, 35 and 40 %). Numerical samples containing **a** 2 % porosity, **b** 20 % porosity and **c** 40 % porosity (all with vesicle diameters from 0.1 to 1.0 mm)

element was damaged and its Young's modulus modified according to the following elastic damage constitutive law (Lemaitre and Chaboche 1990):

$$E = E_0(1-D) \tag{4}$$

where E_0 is the Young's modulus of the damaged element. We note that, although Eq. 4 stipulates that the Young's modulus of an element is 0 GPa when $D=1$ (completely damaged), the programme assigns a value of 1.0×10^{-5} GPa to prevent the system of equations from being ill-posed. The constitutive relations described by Eqs. 3 and 4 are therefore highly dependent on damage parameter D. The following constitutive law can describe the first of the two strength criteria, the maximum tensile strain criterion:

$$D = \begin{cases} 0 & \varepsilon > \varepsilon_{t0} \\ 1-\dfrac{\sigma_{tr}}{\varepsilon E_0} & \varepsilon_{tu} \leq \ \varepsilon \ < \varepsilon_{t0} \\ 1 & \varepsilon < \varepsilon_{tu} \end{cases} \quad (5)$$

where σ_{tr} is the residual uniaxial tensile strength, ε_{tu} is the ultimate tensile strain of the element, and $\sigma_{tr}=\lambda\sigma_{t0}$ (where λ is the residual strength coefficient, and σ_{t0} is the uniaxial tensile strength at the elastic strain limit, ε_{t0}). For the second strength criterion, the Mohr–Coulomb criterion, the damage variable D can be described as follows:

$$D = \begin{cases} 0 & \varepsilon < \varepsilon_{c0} \\ 1-\dfrac{\sigma_{cr}}{\varepsilon E_0} & \varepsilon \geq \varepsilon_{c0} \end{cases} \quad (6)$$

where σ_{cr} is the residual uniaxial compressive strength and is defined as $\sigma_{cr}=\lambda\sigma_{c0}$ (where λ is the residual strength coefficient, and σ_{c0} is the uniaxial compressive strength at the elastic strain limit). During the loading of the numerical sample, the tensile strength criterion was more likely to be met since the tensile strength was set as one tenth of the compressive strength (Table 1; Jaeger et al. 2007). If no elements were damaged in a particular loading increment, the numerical sample was simply subjected to the next 0.002-mm strain increment. However, if any elements were damaged, their Young's moduli were modified according to Eqs. 3 and 4, and the distribution of stress within the sample was recalculated. This process continued until no further elements were damaged. The numerical sample was then subjected to the next 0.002-mm strain increment. This procedure continued until macroscopic sample failure. A flow chart showing the procedure is given as Online Resource 2. We used the number of failed elements in each strain step as a proxy for the acoustic emission (AE) events—transient elastic waves generated by the rapid release of strain energy released during microcracking—that are usually monitored during rock deformation experiments (Lockner 1993). We also therefore monitored the spatial and temporal distribution of AE events during the deformation of the sample.

Results and discussion

Homogeneous vesicle size distribution

Micromechanical modelling

The results of the Sammis and Ashby (1986) pore-emanating crack modelling show that porosity (Fig. 4a) and vesicle size (Fig. 4b) play an important role in dictating brittle strength. An increase in porosity and/or vesicle diameter always results in a reduction in uniaxial compressive strength. The applied stress is concentrated around the vesicle so that the groundmass at the north and south poles of the vesicle are in tension. Vesicle-emanating cracks form within these areas of stress concentration and grow parallel to the direction of the applied macroscopic stress. Cracks that were not neighbours when they were short become neighbours as they grow longer, resulting in crack interaction and further stress magnification. This eventually leads to macroscopic sample failure. It follows that the higher the porosity, the higher the vesicle density (at a constant vesicle size), and therefore, the crack length and the applied macroscopic stress required for crack interaction are reduced. The formulation of Sammis and Ashby (1986) for the stress intensity factor (K_I) at a vesicle-emanating crack tip shows that the stress intensity will be higher when the vesicle diameter is higher (see also Zhu et al. 2010). Since the crack propagates when $K_I=K_{IC}$, the larger the vesicle, the lower the stress required to propagate a crack, explaining the dependence of UCS on the vesicle diameter (at a constant porosity).

The model highlights that the reduction in brittle strength as porosity or vesicle size increases is nonlinear (previously resolved in experimental studies, e.g. Zhu et al. 2010; Baud et al. 2014); the largest reductions are observed at low porosity (Fig. 4a) and small vesicle diameters (Fig. 4b). In detail, the reduction in UCS with increasing porosity is vesicle size dependent. This can be best observed by plotting the rate of UCS reduction against porosity (Fig. 5a). For example, if one were to consider a reduction rate of 2 MPa per 0.1 % porosity increase as the transition between a high and low rate of strength reduction, the porosity of this transition is reduced as vesicle size increases (6.7, 5.3, 4.6, 3.8, 3.0 and 2.4 % for vesicle diameters of 0.1, 0.2, 0.3, 0.5, 1.0 and 2.0, respectively). In other words, below these values, small changes in porosity can produce large changes in strength, and vice versa. The reduction in UCS with increasing vesicle size, however, is only dependent on porosity up to a porosity of about 15 %. Above a porosity of 15 %, the UCS versus vesicle diameter curves all follow approximately the same path (Fig. 4b); the 10, 5 and 2 % porosity curves are progressively offset from these curves (Fig. 4b). The transition to a strength reduction rate of 2 MPa per 0.01-mm diameter increase occurs at vesicle diameters of 0.57, 0.44, 0.37, 0.33, 0.30, 0.29, 0.27, 0.26 and 0.25 mm for porosity values of 2, 5, 10, 15, 20, 25, 30, 35 and 40 %, respectively (Fig. 5b). In other words, above a porosity of 15 %, an increase in vesicle diameter reduces the strength by a similar magnitude regardless of the porosity (up to 40 %). Taken together, we can conclude that vesicle diameter can play an important role in dictating brittle strength at low porosity (as porosity increases, strength is reduced at a higher rate when the vesicle diameter is larger) but is largely inconsequential above 15 % porosity. Vesicle clustering and stress lobe interaction are implicit at high porosity, regardless of the vesicle diameter.

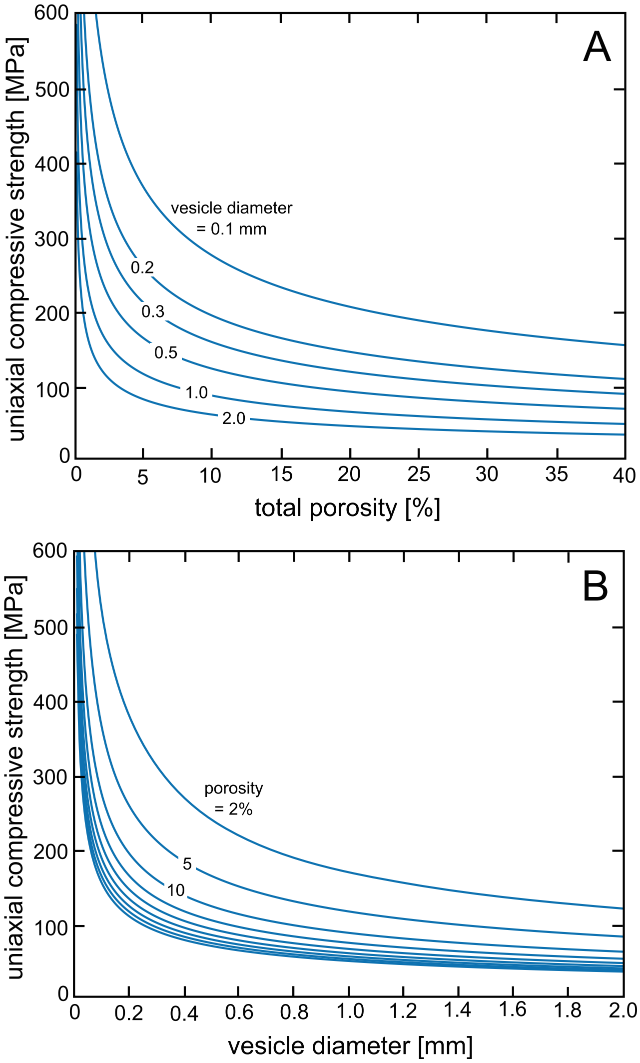

Fig. 4 The results of the Sammis and Ashby (1986) pore-emanating crack modelling. **a** Uniaxial compressive strength against total porosity (up to 40 %) for vesicle diameters of 0.1, 0.2, 0.3, 0.5, 1.0 and 2.0 mm. **b** Uniaxial compressive strength against vesicle diameter (up to 2.0 mm) for porosity values of 2, 5, 10, 15, 20, 25, 30, 35 and 40 %

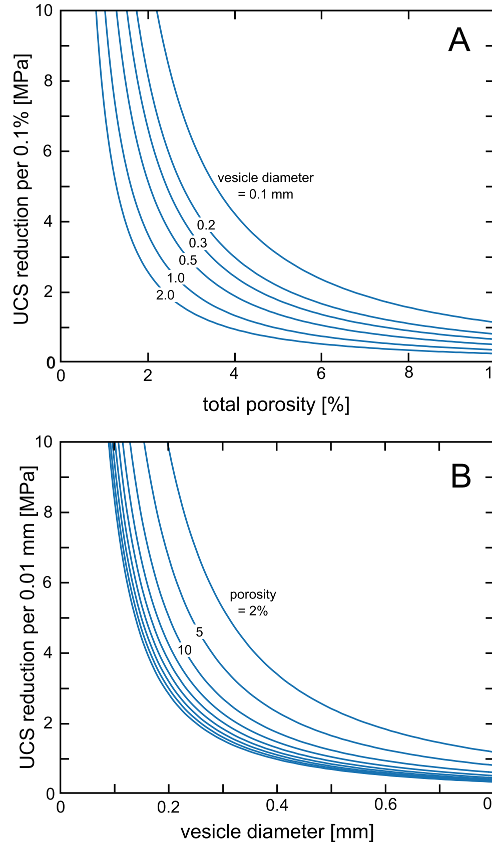

Fig. 5 The results of the Sammis and Ashby (1986) pore-emanating crack modelling. **a** Rate of uniaxial compressive strength reduction per 0.1 % porosity increase against total porosity (up to 40 %) for vesicle diameters of 0.1, 0.2, 0.3, 0.5, 1.0 and 2.0 mm. **b** Rate of uniaxial compressive strength reduction per 0.01-mm vesicle diameter increase against vesicle diameter (up to 2.0 mm) for porosity values of 2, 5, 10, 15, 20, 25, 30, 35 and 40 %

Stochastic modelling

The RFPA stochastic model provides simulated stress–strain curves, an example of one such curve is shown in Fig. 6 (in this case, 2 % porosity and a vesicle diameter of 1 mm). The cumulative AE counts are also shown in Fig. 6. We notice that the stress–strain curve (see Hoek and Bieniawski 1965; Brace et al. 1966; Scholz 1968a) and associated AE activity (see Scholz 1968b) closely matches those typically seen in uniaxial compression experiments in the laboratory. The stress–strain response is first very nearly linear (there is no concave portion typically associated with microcrack closure; our samples do not contain pre-existing microcracks) and represents elastic or recoverable strain accumulation. Beyond a certain stress, about 200 MPa in this case, the curve departs from linearity. This represents the accumulation of permanent damage, the onset of which is contemporaneous with the start of the AE activity (or the failing of elements in the model). The numerical sample eventually fails, marked by a drop in the stress and

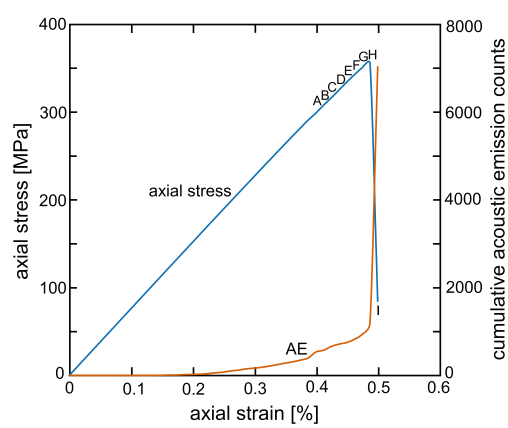

Fig. 6 Uniaxial stress–strain curve, together with the AE activity, for a numerical sample with a homogeneous vesicle size distribution containing 2 % porosity and a vesicle diameter of 1.0 mm. The *letters* next to the stress–strain curve correspond to the stress field and AE snapshots shown in Fig. 7 and Online Resource 3, respectively

a burst of AE activity. In this case, failure occurred at about 356 MPa and after about 0.5 % axial strain. The RFPA model also permits the visualisation of the temporal and spatial evolution of the stress field (Fig. 7) and the AE activity (Online Resource 3). In the stress field snapshots, the greyscale represents the magnitude of the stress: darker colours represent low stresses, and vice versa. Any black areas represent completely damaged elements (D=1). In the AE activity snapshots, each circle represents an AE event. The size of the circle relates to the magnitude of the released energy (larger circles are higher energy events, see Xu et al. 2012 for more details), and the colour relates to the type of event (red for tensile cracks and white for compressive shear cracks). Any black circles represent AE events from a previous calculation step. The stress snapshot at 0.4 % strain (Fig. 7a) shows how the presence of vesicles locally amplifies the stress within the groundmass adjacent to the vesicle. At 0.4 % strain, and as a result of these stress concentration lobes, microcracks are initiated from or near to the vesicle walls (i.e. the weakest elements within the area of stress concentration fail). These failed elements augment the stress on their neighbouring elements and allow microcracks to develop.

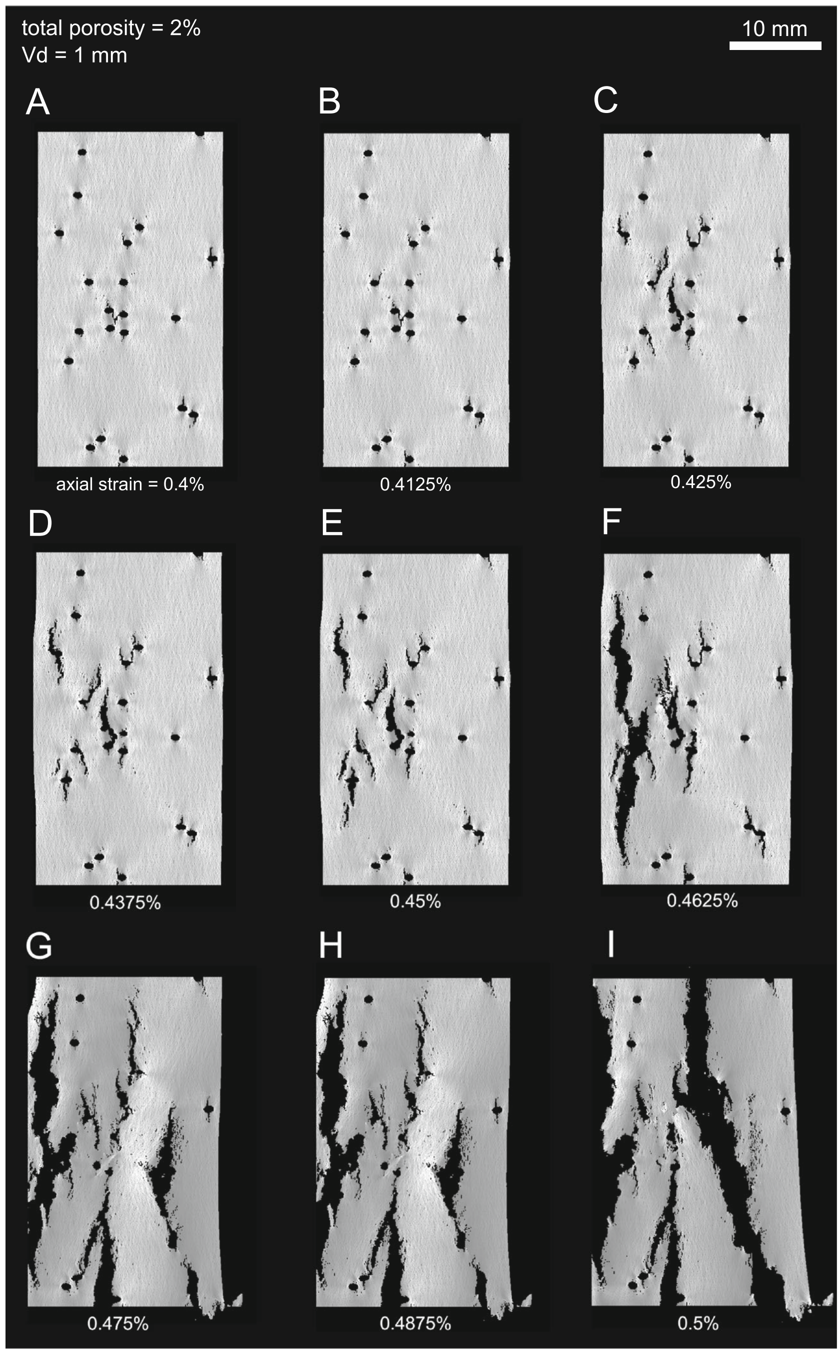

Fig. 7 Stress field snapshots showing the progression of sample failure for the numerical sample with a homogeneous vesicle size distribution (containing 2 % porosity and a vesicle diameter of 1.0 mm) shown in Fig. 6

As strain accumulates in the sample, these microcracks grow and coalesce with other vesicle-emanating microcracks and nearby vesicles. This is most evident in the centre of the sample shown in Fig. 7 where the stress fields of neighbouring vesicles within a vesicle cluster can interact (stress field overlap and interaction further amplify the stress). Eventually, the coalescence of vesicle-emanating microcracks conspires to fail the sample. The AE locations paint a similar story (Online Resource 3). We note that the vast majority of the microcracks are initiated in tension (as typically observed during the failure of rock in compression, see Stanchits et al. (2006)). While we show this numerical sample as an example (it best demonstrates the failure process due to the low porosity and large vesicle diameter), we note that all the simulated samples (regardless of porosity and vesicle size) failed under the same circumstances: the coalescence of vesicle-emanating microcracks.

The model output shows that, similar to the micromechanical modelling, porosity and vesicle size play an important role in dictating rock strength (Fig. 8; Table 2). In detail, an increase in porosity and vesicle diameter reduces brittle strength. The model output is qualitatively similar to those of the micromechanical modelling (Fig. 5). The presence of vesicles locally amplifies the stress within the groundmass (Jaeger et al. 2007; Sammis and Ashby 1986) and promotes the nucleation of vesicle-emanating microcracks that grow, coalesce and eventually lead to macroscopic sample failure (Fig. 7). As porosity increases, not only do the samples contain more void space (meaning that macroscopic failure requires the failure of fewer elements; see Online Resource 4 and Table 2) but also the likelihood of vesicle clustering and stress field overlap and interaction increases. Stress field interaction further magnifies the stress and promotes microcrack initiation and growth and ultimately sample failure, at lower applied stresses. Vesicles with a larger diameter magnify the stress of a larger area (perturbations in the stress field can be considered negligible at distances greater than ten times the diameter; Jaeger et al. 2007). This may imply that, at constant porosity, larger vesicles create more stress field overlap than smaller vesicles or that the fewer, larger stress concentration lobes of the larger vesicles increase the likelihood that weaker elements are found within the area of stress concentration. However, the model also shows that, at constant porosity, failure requires the failure of fewer elements when the vesicle diameter is larger (Online Resource 4 and Table 2); larger vesicles permit a shorter route through the groundmass for the macroscopic shear fracture.

The modelled output of Fig. 8b shows, similar to the micromechanical modelling of Fig. 5b, that the curves for the samples containing porosity values lower than 15 % are increasingly offset from those above 15 %. As explained above, the model output suggests that, below a porosity of 15 %, vesicle diameter plays an important role in dictating

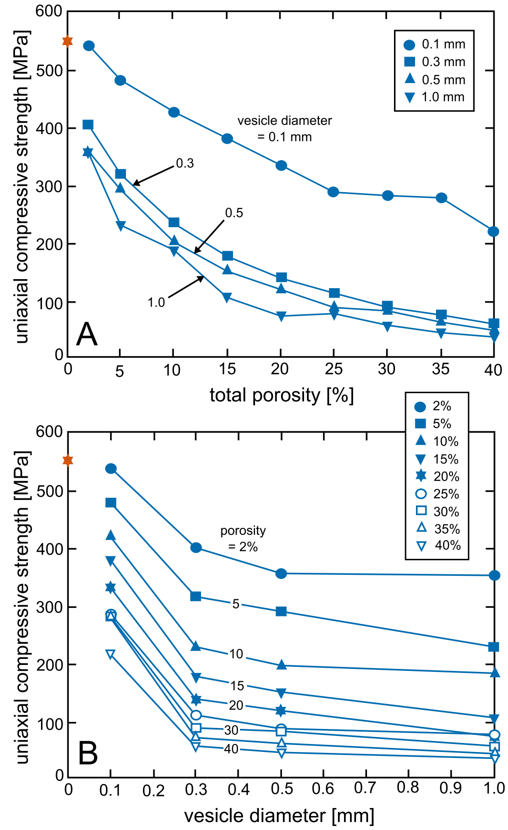

Fig. 8 The results of the rock failure and process analysis (RFPA) code stochastic modelling for samples with a homogeneous vesicle size distribution. **a** Uniaxial compressive strength against total porosity (up to 40 %) for vesicle diameters of 0.1, 0.3, 0.5 and 1.0 mm. **b** Uniaxial compressive strength against vesicle diameter (up to 1.0 mm) for porosity values of 2, 5, 10, 15, 20, 25, 30, 35 and 40 %. The strength of a sample containing 0 % is represented by the *red stars*

brittle strength. The stress fields of neighbouring vesicles can easily interact above a porosity of 15 %, regardless of their diameter, due to their proximity at high porosity.

The number of AEs (Online Resource 4) and the axial strain (Online Resource 5) required for brittle failure also decrease as porosity and vesicle diameter increase (see also Table 2). The number of AEs required for brittle failure falls from about 11,500 hits (2 % porosity and 0.1-mm vesicles) to about 1,500 hits (40 % porosity and 1.0-mm vesicles). Axial strains of about 0.75 % are required for failure at low porosity values and small vesicle diameters, whereas, for high porosity values and large vesicle diameters, strain at failure can be as low as 0.3 %. We also highlight that the curves for the number of AEs (Online Resource 4) and the axial strain (Online Resource 5) required for failure are very similar for samples containing a porosity of 15 % or higher, regardless of the vesicle diameter. It follows that samples with the same strength should fail at similar strains and numbers of AEs.

An increase in porosity also serves to dramatically reduce Young's modulus, from just below 80 GPa at 2 % to as low as

Table 2 Model output summary for all of the RFPA simulations performed in this study

Total porosity (%)	Vesicle diameter (mm)	Peak stress (MPa)	Strain at failure (%)	Young's modulus (GPa)	Acoustic emissions required for failure
0	N/A	553.5	0.7375	80.8	10,018
2	0.1	543.2	0.7500	78.6	11,576
2	0.3	426.9	0.6000	76.0	8,568
2	0.3	382.5	0.5500	75.7	6,697
2	0.5	358.2	0.5000	75.7	6,936
2	1.0	355.6	0.5000	76.0	7,032
2	0.1; 0.3	484.5	0.6750	77.2	9,854
2	0.1; 0.5	433.5	0.6000	77.1	8,462
2	0.1; 1.0	374.0	0.5125	76.9	7,783
5	0.1	482.3	0.6750	76.2	8,332
5	0.3	333.3	0.5250	69.3	6,939
5	0.3	303.5	0.4750	69.1	3,827
5	0.5	291.2	0.4625	69.0	6,870
5	1.0	229.8	0.4125	68.2	5,783
10	0.1	427.1	0.6500	71.3	11,000
10	0.3	229.9	0.4375	59.3	5,639
10	0.3	235.5	0.4375	58.9	4,854
10	0.5	200.1	0.3875	58.1	4,470
10	1.0	186.2	0.4375	58.8	4,441
15	0.1	330.5	0.6125	66.2	6,947
15	0.3	182.2	0.3750	50.0	5,788
15	0.3	168.6	0.3750	50.0	3,326
15	0.5	149.1	0.3375	50.4	2,555
15	1.0	103.4	0.3000	48.5	2,958
20	0.1	333.9	0.5750	63.3	5,124
20	0.3	134.9	0.3750	42.0	2,846
20	0.3	140.0	0.3875	41.9	3,933
20	0.5	117.4	0.3125	42.2	2,375
20	1.0	71.6	0.3000	39.7	2,489
25	0.1	287.0	0.5125	59.6	5,649
25	0.3	109.9	0.3625	34.9	2,180
25	0.3	112.3	0.4000	35.2	3,144
25	0.5	86.2	0.2875	34.5	1,808
25	1.0	75.8	0.3250	34.3	2,545
30	0.1	281.0	0.5375	56.4	5,451
30	0.3	84.8	0.4000	28.5	3,427
30	0.3	89.4	0.3875	29.0	3,340
30	0.5	80.6	0.3500	29.0	2,968
30	1.0	55.6	0.2625	27.0	1,912
35	0.1	277.5	0.5250	56.6	5,567
35	0.3	74.8	0.3625	23.8	2,816
35	0.3	71.6	0.3875	23.5	2,328
35	0.5	60.6	0.3125	23.7	1,740
35	1.0	42.3	0.2500	22.2	1,654
40	0.1	219.3	0.4750	50.7	6,174
40	0.3	54.3	0.3375	18.7	1,311
40	0.3	60.9	0.4125	18.8	2,841
40	0.5	46.5	0.3125	19.0	1,394
40	1.0	35.0	0.2375	17.9	1,313
40	0.1; 0.3	92.3	0.3625	29.2	3,044
40	0.1; 0.5	77.9	0.3000	29.9	1,982
40	0.1; 1.0	54.8	0.2500	27.3	1,460

about 20 GPa at 40 % (Online Resource 6 and Table 2). We note that the Young's modulus–porosity curves follow the same path at vesicle diameters of 0.3 mm and above, suggesting that an increase in vesicle diameter above 0.3 mm (at constant porosity) does not influence the Young's modulus.

Inhomogeneous vesicle size distribution

We performed a series of pilot simulations, using the RFPA stochastic model, in which we populated the sample with vesicles of two different diameters. The motivation behind these simulations was to see whether the strength of the sample containing two vesicle size populations would be closer to that of the smallest vesicle diameter (i.e. 0.1 mm) or the largest vesicle diameter (0.3, 0.5 or 1.0 mm). The results are shown as Fig. 9. The blue bars represent the small-diameter end-member (0.1 mm), the green bars represent the large-diameter end-member (0.3, 0.5 or 1.0 mm), and the red bars represent an equal (in area) mixture of the two end-members. The histograms of Fig. 9 show that the strengths of the samples containing an inhomogeneous vesicle size distribution (the red bars) are much closer to the strengths of the large-vesicle-diameter end-members (the green bars). Therefore, the large vesicles are dictating the strength of the sample. To illustrate why this is the case, one only needs to look at the snapshots showing the progression of damage accumulation in the samples. Two examples are presented as Fig. 10. Figure 10 shows that the 0.1-mm vesicles, although equal in area to the larger vesicles (and therefore greater in number), only influence the stress in their immediately adjacent elements, limiting stress field interaction. By contrast, the larger vesicles have a much broader impact and influence the stress on many elements, increasing the probability of stress field interaction (see, for example, the first snapshot of Fig. 10a). As strain accumulates in the samples, the vesicle-emanating microcracks grow from the large vesicles; eventually, their growth and coalesce result in macroscopic sample failure. We note that, since an inhomogeneous vesicle size

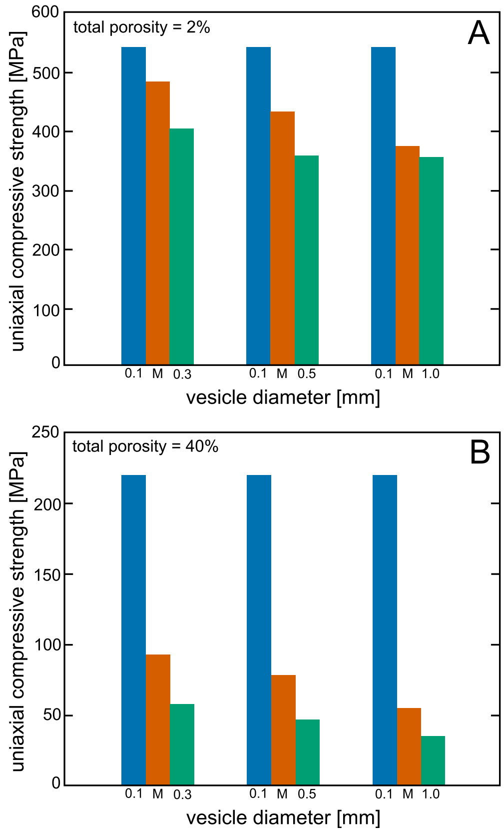

Fig. 9 The results of the RFPA numerical modelling for the samples with an inhomogeneous vesicle size distribution. **a** Histogram showing the modelled uniaxial compressive strengths for samples with a homogeneous vesicle size distribution with porosity of 2 % and vesicle sizes of 0.1 mm (*blue bars*) and 0.3, 0.5 or 1.0 mm (*green bars*) and samples with an inhomogeneous vesicle size distribution with porosity of 2 % and an equal area of 0.1-mm vesicles and 0.3, 0.5 or 1.0-mm vesicles (*red bars*, labelled 'M'). **b** The same as in **a** but for samples containing porosity of 40 %

distribution is a more realistic scenario in nature, future efforts should be focused in this direction.

Volcanological significance

Volcanic rocks

The residual porosity and diameter of the preserved vesicles, and their diameter size distribution, in volcanic rock depend on the attributes of the magma from which they form (e.g. melt viscosity and magma volatile content and type; Gonnermann and Manga 2012 and references therein) and its eruptive history (e.g. decompression rate; Gondé et al. 2011; Gonnermann and Manga 2012 and references therein). Experimental studies on volcanic rocks have shown that strength decreases as the porosity increases (e.g. Al-Harthi et al. 1999; Heap et al. 2014). Our modelled output agrees with this observation and also offers insight into the role of vesicle size on brittle strength.

Viewed simplistically, conditions that favour the formation of rocks with high porosity and/or large vesicle diameters (e.g. explosive volcanoes) will deposit volcanic strata with a low brittle strength, and vice versa (e.g. effusive volcanoes). Explosive volcanoes that persistently erupt high-porosity volcanic rocks with large vesicle diameters may therefore erect structurally unstable edifices that could be susceptible to devastating flank collapse (e.g. Voight and Elsworth 2000). However, volcanoes typically switch between explosive (high-porosity products) and effusive (low-porosity products) activity, and can have rapidly evolving ascent rates and outgassing efficiency, and are therefore more likely to construct an edifice comprising layers of rock containing very different porosity values and vesicle diameters. Our modelling has shown that porosity and vesicle diameter can severely doctor the strength (Fig. 4) and Young's modulus (Online Resource 6). Stratovolcanoes, constructed from alternating layers of rock with different Young's moduli and strengths (as depicted in Fig. 11), will promote the arrest or deflection of propagating dykes and fractures thereby increasing the strain energy required for large-scale failure (e.g. Gudmundsson 2009, 2012). A summary diagram, showing the evolution of strength, Young's modulus, strain at failure and acoustic emissions required for brittle failure in lava strata containing variable porosity/vesicle sizes, is given as Fig. 11.

Magma

If melts are deformed at strain rates in excess of the inverse of their relaxation timescale, then the melt phase will behave as a solid (Dingwell and Webb 1990; Dingwell 1996). For example, the fragmentation of silicic melts has been observed experimentally during rapid decompression (e.g. Martel et al. 2000). The purely brittle response of melt is exemplified by the similarity between fragmentation data obtained at 25 and 850 °C (e.g. Mueller et al. 2008). Numerical modelling has shown that the shear strain rate within the conduit increases from the centre to the margin; shear strain rates also increase with increasing ascent distance, expanding the brittle field at the conduit margins (e.g., Gonnermann and Manga 2003; Fig. 12). The model of Gonnermann and Manga (2003) demonstrated that the melt near the conduit would eventually be subjected to shear strain rates that exceed their structural relaxation timescale. We reiterate that our modelling can only be applied to the magma within these narrow zones; the magma in the centre of the conduit will deform viscously. Further, our modelling only considers two-phase brittle magma (i.e. melt and vesicles) in which the vesicles do not contain an overpressure. It is likely that the transition to a brittle response will be met at lower bulk strain rates in the presence of crystals (e.g. Lavallée et al. 2007; Cordonnier et al. 2012; Kendrick et al. 2013) or bubble overpressures.

Fig. 10 Stress field snapshots showing the progression of sample failure for two numerical samples with inhomogeneous vesicle size distributions, one containing 2 % porosity and vesicle diameters of 0.1 and 1.0 mm (a) and one containing 2 % porosity and vesicle diameters of 0.1 and 0.5 mm (b)

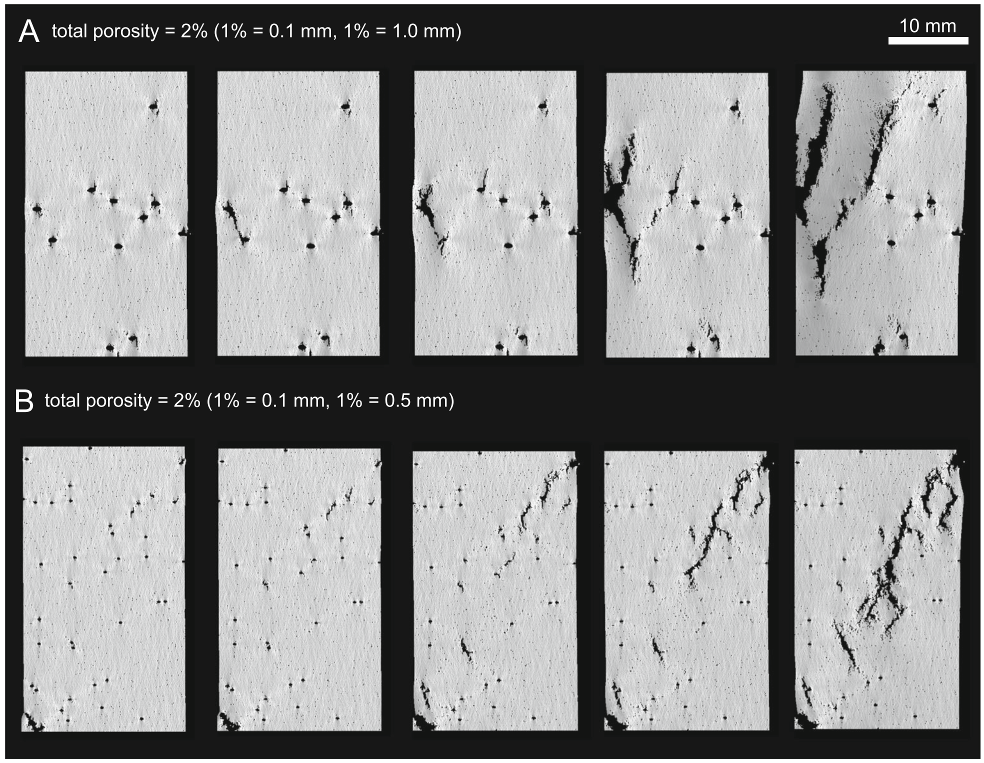

Since the volatiles contained within the magma are less soluble as the magma depressurises on its way to the surface, it is likely therefore that vesicle size, porosity or both vesicle size and porosity will increase as distance to the surface decreases (e.g. Gonnermann and Manga 2012). We have depicted two scenarios in Fig. 12: one in which the vesicle size increases with height in the conduit (Fig. 12a) and another in which porosity increases with height in the conduit (Fig. 12b). These end-member scenarios, represented as cartoons, show the areas of the conduit likely to experience brittle deformation (dark grey) and those areas likely to deform viscously (light grey), governed by the inhomogeneous distribution of strain rate within the conduit (illustrated by the graph between the cartoons, Gonnermann and Manga 2003). The brittle strength curves for increasing vesicle size and porosity, taken from the micromechanical modelling (Fig. 4), are shown next to the appropriate cartoon. The modelled output suggests that, for a constant porosity (Fig. 12a) or vesicle size (Fig. 12b), the brittle strength at the conduit margins will decrease significantly as distance to the surface decreases. We also note that our stochastic modelling suggests that the strain (Online Resource 5) and acoustic emission hits (Online Resource 4) required for brittle failure will decrease as distance to the surface decreases. In nature, a much more likely scenario is that vesicle size and porosity both increase as distance to the surface decreases (i.e. a scenario between these two end-members). We have represented this scenario as a dashed red line on each graph. We note that the red line follows the same trajectory as the UCS-total porosity data for porous magma presented in Vasseur et al. (2013). Our modelled output illustrates, depending on the attributes of the magma, how brittle strength can deviate from this idealised curve. For instance, for a given volume of volatiles, if the bubbles can coalesce with a greater ease (perhaps their

Fig. 11 Summary diagram showing the evolution of brittle strength, Young's modulus, strain at failure and acoustic emissions required for brittle failure in lava strata containing variable porosity/vesicle sizes

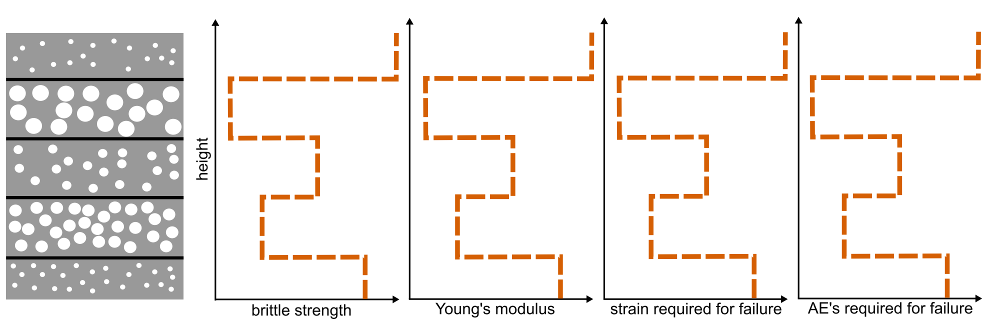

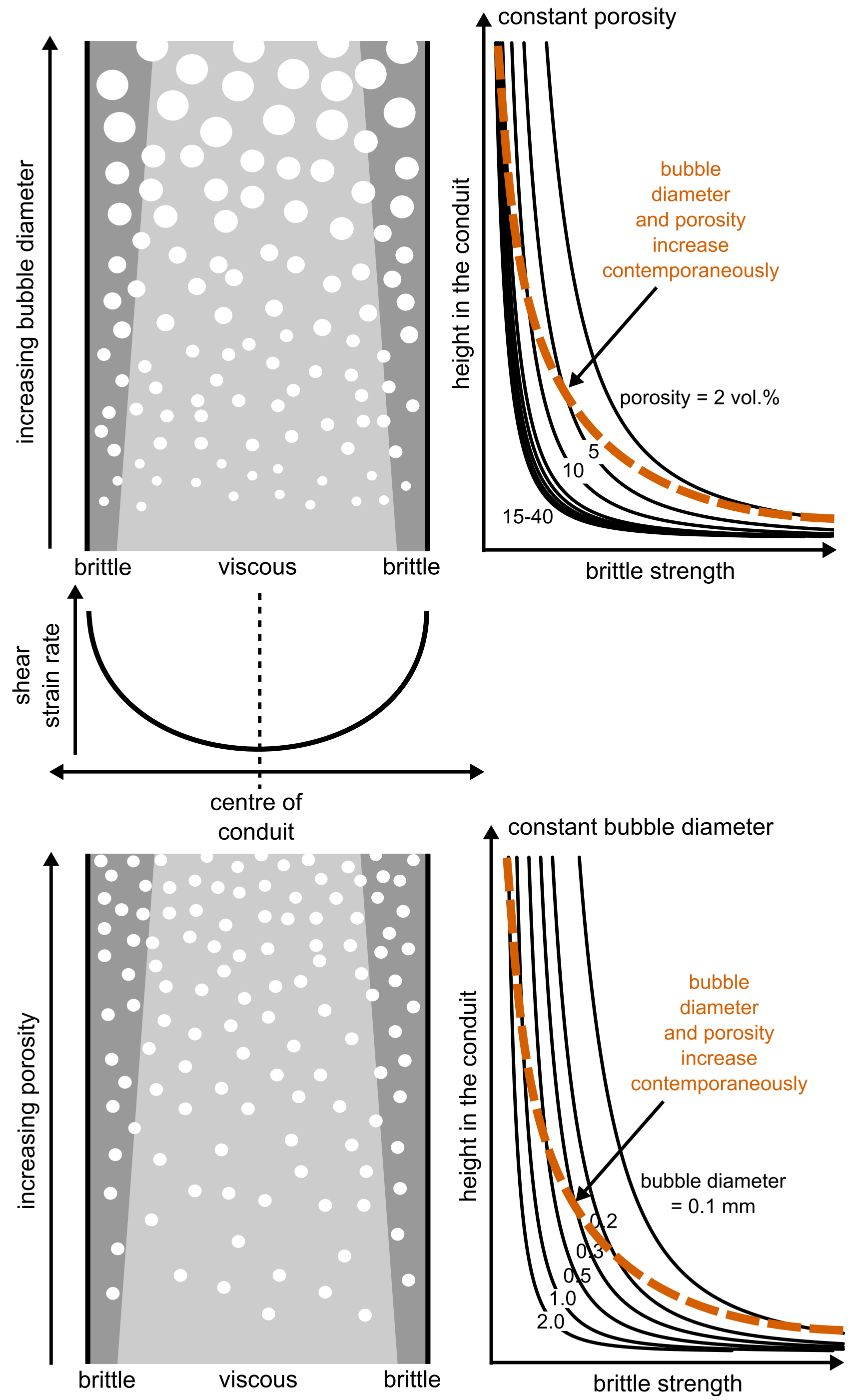

Fig. 12 Cartoons of magma conduits showing scenarios in which vesicle diameter increases (**a**) and porosity increases (**b**) as distance to the surface decreases. The cartoons show the areas expected to behave in a viscous (*light grey*) and a brittle (*dark grey*) manner (Gonnermann and Manga 2003). Brittle strength curves (from the micromechanical modelling of Fig. 4) are provided for each cartoon (see text for details)

movement is not restricted by a high crystal content, or the viscosity is low and allows for efficient bubble migration and coalescence), then the magma will have a considerably lower brittle strength. This huge reduction in strength can occur in low-porosity magma far from the surface (Fig. 12b). Similarly, magma containing high volatile contents, or magma that is unable to efficiently outgas, can have high porosity values and therefore low brittle strengths. Strong magma requires low porosity values and small vesicle diameters.

The brittle failure of magma at the conduit boundary is likely to increase its permeability (e.g. Laumonier et al. 2011; Kolzenburg et al. 2014; Lavallée et al. 2013; Kendrick et al. 2013). The ease at which volatiles can escape through the side of the conduit into the host rock (Jaupart 1998), or along conduit faults to the surface (Lavallée et al. 2013), can promote or diffuse explosivity (e.g. Mueller et al. 2008). Therefore, magma with large vesicles and/or high porosities (that have low brittle strengths as a result), may aid outgassing and reduce eruption explosivity, and vice versa.

Concluding remarks and perspectives

This contribution presents the results of modelling designed to shed light on the influence of porosity and vesicle size on the brittle strength of volcanic rocks and magma. We find that porosity and vesicle size play an important role in governing brittle strength. An increase in porosity and/or vesicle diameter results in a reduction of uniaxial compressive strength. Vesicles generate tensile stress concentration lobes within the groundmass. Microcracks preferentially nucleate within these zones and propagate towards the direction of the macroscopic applied stress. Eventually, vesicle-emanating microcracks interact, coalesce and promote macroscopic failure. Vesicle clustering (allowing stress concentration lobes of neighbouring vesicles to overlap) and an increase in the ease of microcrack interaction reduce the strength at higher porosity (at a constant vesicle size). Larger vesicles lower the macroscopic applied stress required to propagate vesicle-emanating microcracks, explaining the reduction in strength at higher vesicle diameters (at constant porosity). The models demonstrate that the reduction in strength as porosity or vesicle size increases is nonlinear (a trend previously resolved through experimentation); the largest reductions are observed at low porosity and small vesicle diameters. In detail, vesicle diameter can play an important role in dictating strength at low porosity but is largely inconsequential above 15 % porosity. Regardless of the vesicle diameter, vesicle clustering and stress field overlap are unavoidable at high porosity. Samples containing a bimodal vesicle size distribution are closer to the strength of the largest vesicle size end-member; indeed, vesicle-emanating microcracks first nucleate from the largest vesicles.

The implications of these results are that highly porous lava and magma with high vesicle diameters will have low brittle strengths. Persistently explosive (high-porosity products) and effusive (low-porosity products) volcanoes may construct weak and strong edifices, respectively. Weak edifice-forming lava may leave the edifice more susceptible to large-scale failure. However, stratovolcanoes built from successive explosive and effusive eruptions may be strong as alternating weak and strong layers may promote fracture and dyke arrest. Magma containing high porosity values and large vesicle diameters may suffer brittle fracture more readily at the conduit boundary where it can behave in a brittle manner. This could increase permeability, facilitate outgassing and reduce the eruption explosivity.

We highlight that the variety in the microstructure of volcanic rocks and magma is extremely wide. We have not, in this contribution, considered a complete description. For instance, we have not considered crystals, bubble overpressures or variations in vesicle shape. Our modelling approach does, however, offer valuable insights and a basis for future studies using these models, largely unused in volcanology at present. Forthcoming efforts will focus on the influence of bubble overpressure and crystal content.

Acknowledgments The idea for this paper was inspired by the comments of an anonymous reviewer. The authors of this study acknowledge the support of a Partenariats Hubert Curien (PHC) Xu Guangqi grant (grant number 32195NC), managed by Campus France and supported by the Ministry of Foreign Affairs (MAE) in France and the French Institute of the Chinese Embassy of France in China. Tao Xu acknowledges the National Natural Science Foundation of China (grant number 51474051). This work has benefitted from discussions with Kelly Russell, Patrick Baud, Alexandra Kushnir, Jamie Farquharson, Fabian Wadsworth, Nicolas Brantut, and Olivier Lengliné. We would like to thank Jackie Kendrick, Jérémie Vasseur and the editor, August Gudmundsson, for helpful comments and suggestions that improved this manuscript.

References

Al-Harthi AA, Al-Amri RM, Shehata WM (1999) The porosity and engineering properties of vesicular basalt in Saudi Arabia. Eng Geol 54:313–320

Amitrano, D., and A. Helmstetter (2006), Brittle creep, damage, and time to failure in rocks, J Geophys Res 111. doi:10.1029/2005JB004252

Baud P, Wong T-F, Zhu W (2013) Effects of porosity and crack density on the compressive strength of rocks. Int J Rock Mech Min. doi:10.1016/j.ijrmms.2013.1008.1031, In press

Baud P, Wong T-F, Zhu W (2014) Effects of porosity and crack density on the compressive strength of rocks. Int J Rock Mech Min. doi:10.1016/j.ijrmms.2013.1008.1031, In press

Brace WF, Paulding BW, Scholz CH (1966) Dilatancy in the fracture of crystalline rocks. J Geophys Res 71:3939–3953

Caricchi L, Pommier A, Pistone M, Castro J, Burgisser A, Perugini D (2011) Strain-induced magma degassing: insights from simple-shear experiments on bubble bearing melts. Bull Volcanol 73:1245–1257

Chang C, Zoback MD, Khaksar A (2006) Empirical relations between rock strength and physical properties in sedimentary rocks. J Pet Sci Eng 51:223–237

Cordonnier B, Caricchi L, Pistone M, Castro J, Hess K-U, Gottschaller S, Manga M, Dingwell DB, Burlini L (2012) The viscous-brittle transition of crystal-bearing silicic melt: direct observation of magma rupture and healing. Geology 40:611–614

Dingwell DB (1996) Volcanic dilemma–flow or blow? Science 273:1054–1055

Dingwell DB, Webb SL (1990) Relaxation in silicate melts. Eur J Mineral 2:427–449

Fakhimi A, Gharahbagh EA (2011) Discrete element analysis of the effect of pore size and pore distribution on the mechanical behavior of rock. Int J Rock Mech Min 48:77–85

Gondé C, Martel C, Pichavant M, Bureau H (2011) In situ bubble vesiculation in silicic magmas. AM Mineral 96:111–124

Gonnermann HM, Manga M (2003) Explosive volcanism may not be an inevitable consequence of magma fragmentation. Nature 426:432–435

Gonnermann, H. M., and M. Manga (2012), Dynamics of magma ascent in the volcanic conduit. In Fagents SA, GTKP, Lopes RMC (eds) Modeling volcanic processes: the physics and mathematics of volcanism. Cambridge University Press, Cambridge.

Gudmundsson A (2009) Toughness and failure of volcanic edifices. Tectonophysics 471:27–35

Gudmundsson A (2012) Strengths and strain energies of volcanic edifices: implications for eruptions, collapse calderas, and landslides. Nat Hazards Earth Syst Sci 12:2241–2258

Heap MJ, Lavallée Y, Petrakova L, Baud P, Reuschlé T, Varley N, Dingwell DB (2014) Microstructural controls on the physical and mechanical properties of edifice-forming andesites at Volcán de Colima, Mexico. J Geophys Res 119:2925–2963

Hoek E, Bieniawski ZT (1965) Brittle fracture propagation in rock under compression. Int J Fract 1:137–155

Jaeger J, Cook NGW, Zimmerman R (2007) Fundamentals in rock mechanics, 4th edn. Blackwell Publishing, London

Jaupart C (1998) Gas loss from magmas through conduit walls during eruption. Geol Soc Lond, Spec Publ 145:73–90

Kendrick JE, Lavallée Y, Hess K-U, Heap MJ, Gaunt HE, Meredith PG, Dingwell DB (2013) Tracking the permeable porous network during strain-dependent magmatic flow. J Volcanol Geotherm Res 260: 117–126

Kolzenburg S, Heap MJ, Lavallée Y, Russell JK, Meredith PG, Dingwell DB (2014) Strength and permeability recovery of tuffisite-bearing andesite. Solid Earth 3:191–198

Kueppers U, Scheu B, Spieler O, Dingwell DB (1995) Field-based density measurements as tool to identify preeruption dome structure: set-up and first results from Unzen volcano, Japan. J Volcanol Geotherm Res 141:65–75

Lacroix P, Amitrano D (2013) Long-term dynamics of rockslides and damage propagation inferred from mechanical modeling. J Geophys Res 118:2292–2307

Laumonier M, Arbaret L, Burgisser A, Champallier R (2011) Porosity redistribution enhanced by strain localisation in crystal-rich magmas. Geology 39:715–718

Lavallée Y, Hess K-U, Cordonnier B, Dingwell DB (2007) A non-Newtonian rheological flow law for highly-crystalline dome lavas. Geology 35:843–846

Lavallée Y, Benson PM, Heap MJ, Hess K-U, Flaws A, Schillinger B, Meredith PG, Dingwell DB (2013) Reconstructing magma failure and the degassing network of dome-building eruptions. Geology 41: 515–518

Lemaitre J, Chaboche J-L (1990) Mechanics of solid materials. Cambridge University Press, Cambridge

Liu D-M (1997) Influence of porosity and pore size on the compressive strength of porous hydroxyapatite ceramic. Ceram Int 23:135–139

Lockner D (1993) The role of acoustic emission in the study of rock fracture. Int J Rock Mech Min Sci Geomech Abstr 30(7):883–889

Mangan M, Cashman KVN (1993) Vesiculation of basaltic magma during eruption. Geology 21:157–160

Martel C, Dingwell DB, Spieler O, Pichavant M, Wilke M (2000) Fragmentation of foamed silicic melts: an experimental study. Earth Planet Sci Lett 178:47–58

Martel C, Dingwell DB, Spieler O, Pichavant M, Wilke M (2001) Experimental fragmentation of crystal- and vesicle-bearing silicic melts. Bull Volcanol 63:398–405

Mueller S, Scheu B, Spieler O, Dingwell DB (2008) Permeability control on magma fragmentation. Geology 36:399–402

Navon O, Lyakhovsky V (1998) Vesiculation processes in silicic magmas. Geol Soc Lond, Spec Publ 145:27–50

Pistone M, Caricchi L, Ulmer P, Burlini L, Ardia P, Reusser E, Marone F, Arbaret L (2012) Deformation experiments of bubble- and crystal-bearing magmas: rheological and microstructural analysis. J Geophys Res 117, B05208. doi:10.1029/2011JB008986

Reid ME, Keith TEC, Kayan RE, Iverson NR, Iverson RM, Brien DL (2010) Volcano collapse promoted by progressive strength reduction: new data from Mount St. Helens. Bull Volcanol 72:761–766

Sammis CG, Ashby MF (1986) The failure of brittle porous solids under compressive stress states. Acta Metall Mater 34:511–526

Scholz CH (1968a) Microfracturing and the inelastic deformation of rock in compression. J Geophys Res 73:1417–1432

Scholz CH (1968b) Microfractures, aftershocks, and seismicity. Bull Seismol Soc Am 58:1117–1130

Shea T, Houghton BF, Gurioli L, Cashman KV, Hammer JE, Hobden BJ (2010) Textural studies of vesicles in volcanic rocks: an integrated methodology. J Volcanol Geotherm Res 190: 271–289

Sparks RSJ (1978) The dynamics of bubble formation and growth in magmas: a review and analysis. J Volcanol Geotherm Res 3:1–37

Spieler O, Kennedy B, Kueppers U, Dingwell DB, Scheu B, Taddeucci J (2004) The fragmentation threshold of pyroclastic rocks. Earth Planet Sci Lett 226:139–148

Stanchits S, Vinciguerra S, Dresen G (2006) Ultrasonic velocities, acoustic emission characteristics and crack damage of basalt and granite. Pure Appl Geophys 163:974–993

Tang CA (1997) Numerical simulation of progressive rock failure and associated seismicity. Int J Rock Mech Min 34:249–261

Tang CA, Huang ML, Zhao XD (2003) Weak zone related seismic cycles in progressive failure leading to collapse in brittle crust. Pure Appl Geophys 160:2319–2328

Toramaru A (1989) Vesiculation process and bubble size distributions in ascending magmas with constant velocities. J Geophys Res 94(B12):17523–17542

Vasseur J, Wadsworth FB, Lavallée Y, Hess K-U, Dingwell DB (2013) Volcanic sintering: timescales of viscous densification and strength recovery. Geophys Res Lett 40:5658–5664

Voight B (2000) Structural stability of andesite volcanoes and lava domes. Causes consequences eruptions andesite volcanoes. Philos T Roy Soc A 358(1770):1663–1703

Voight B, Elsworth D (2000) Instability and collapse of hazardous gas-pressurized lava domes. Geophys Res Lett 27:1–4

Weibull W (1951) A statistical distribution function of wide applicability. J Appl Mech 18:293–297

Wiederhorn SM (1969) Fracture surface energy of glass. J Am Ceram Soc 52(2):99–105

Wong T-F, Baud P (2012) The brittle-ductile transition in rocks: a review. J Struct Geol 44:25–53

Wong T-F, Wong RHC, Chau KT, Tang CA (2006) Microcrack statistics, Weibull distribution and micromechanical modeling of compressive failure in rock. Mech Mater 38:664–681

Wright HMN, Cashman KV, Gottesfeld EH, Roberts JJ (2009) Pore structure of volcanic clasts: measurements of permeability and electrical conductivity. Earth Planet Sci Lett 280:93–104

Xu T, C-A Tang (2008) Modeling of stress-induced permeability evolution and damage of rock, Adv Mater Res 33–37: 609–616

Xu T, Tang CA, Yang TH, Zhu WC, Liu J (2006) Numerical investigation of coal and gas outbursts in underground collieries. Int J Rock Mech Min 43:905–919

Xu T, Tang C-A, Zhao J, Li L, Heap MJ (2012) Modelling the time-dependent rheological behaviour of heterogeneous brittle rocks. Geophys J Int 189:1781–1796

Xu XH, Ma SP, Xia MF, Ke FJ, Bai YL (2004) Damage evaluation and damage localization of rock. Theor Appl Fract Mech 42: 131–138

Zhang Y (1999) A criterion for the fragmentation of bubbly magma based on brittle failure theory. Nature 402:648–650

Zhu W, Baud P, Wong T-F (2010) Micromechanics of cataclastic pore collapse in limestone. J Geophys Res. doi:10.1029/2009JB006610

Zhu W, Baud P, Vinciguerra S, Wong T-F (2011) Micromechanics of brittle faulting and cataclastic flow in Alban Hills tuff, J Geophys Res 116 (B06209). doi:06210.01029/02010JB008046.